Nurul Fazlin Roslan, Alvaro Luna, Joan Rocabert, Ignacio Candela, Pedro Rodríguez. (2018) Remote power control strategy based on virtual flux approach for the grid tied power converters. ECCE 2018: IEEE Energy Conversion Congress and Exposition: Portland, OR, USA: Sept. 23-27, 2018: IEEE, 2018. Pp. 7114-7120 Doi: 10.1109/ECCE.2018.8557661.

Nurul Fazlin Roslan, Alvaro Luna, Joan Rocabert, Ignacio Candela, Pedro Rodríguez. (2018) Remote power control strategy based on virtual flux approach for the grid tied power converters. ECCE 2018: IEEE Energy Conversion Congress and Exposition: Portland, OR, USA: Sept. 23-27, 2018: IEEE, 2018. Pp. 7114-7120 Doi: 10.1109/ECCE.2018.8557661.

Remote Power Control Strategy based on Virtual Flux Approach for the Grid Tied Power Converters

Nurul Fazlin Roslan
Department of Electrical Engineering, Technical University of Catalonia, Research Center on Renewable Electrical Energy Systems (SEER)
Barcelona, Spain.
nurulfazlin@unikl.edu.my

Alvaro Luna
Department of Electrical Engineering, Technical University of Catalonia, Research Center on Renewable Electrical Energy Systems (SEER)
Barcelona, Spain.
luna@ee.upc.edu

Joan Rocabert
Department of Electrical Engineering, Technical University of Catalonia, Research Center on Renewable Electrical Energy Systems (SEER)
Barcelona, Spain.
rocabert@ee.upc.edu

Jose Ignacio Candela
Department of Electrical Engineering, Technical University of Catalonia, Research Center on Renewable Electrical Energy Systems (SEER)
Barcelona, Spain.
candela@ee.upc.edu

Pedro Rodriguez
Department of Engineering, Loyola University of Andalusia
Seville, Spain
prodriguez@uloyola.es

***Abstract*—The control of active and reactive power for the Renewable Energy Sources (RES) based power plants are very important. The injection of active and reactive power to the grid is normally controlled at the Point of Common Connection (PCC) where this point is typically far away from the power converter station. This paper proposed a controlling principle which is based on virtual flux approach that permits to control remotely the power injected at the PCC. The results will show that the Virtual Flux (VF) estimation is capable to estimate the grid voltage in any point of the network as well as the capability of the control principle to inject the specific amount of active and reactive power at a point that can be some kilometers away. In this paper, the basic principle for the remote power control is presented and the effectiveness of the proposed system has been validated by experimental studies.**

Keywords— ***Voltage Sensorless, Virtual Flux Estimation, Voltage Source Converter, Proportional Resonant Current Controller, LCL-Filter, Remote Point***

I. INTRODUCTION

The penetration of photovoltaic (PV) and wind-generated electrical energy into the grid system are increased and rapidly developed. According to the International Renewable Energy Agency Report 2017 [1] (p. 18), the wind and PV energy system leads the ranking of renewable energy capacity installation in 2015. In the grid integration of wind and PV systems, the power converters and its controllability are the key element for attaining an efficient control.

The grid synchronization lies in the accurate detection of the attributes of the grid voltage and this can be done by direct measurement of the grid voltage [2] or by implementing a voltage sensorless [3] control solution. In the voltage sensorless control application, the Voltage Oriented Control (VOC) and the Direct Power Control (DPC) approaches are usually applied in the control system. One of the simplest way to achieve the voltage sensorless control is by implementing the VF approach where in this case, the grid voltage condition has been determined by an estimation [4] and the control strategies also can be done in both VOC or DPC. In [5, 6], a comparison between the voltage based control with the VF based control both working in DPC and VOC were presented. A dual virtual flux model was implemented in [7], where the implementation of the model is based on two cascaded low pass filters performed in the stationary reference frame.

The works proposed in [8, 9] are presented with the determination to improve the dynamic performance by taking into consideration the Dual Second Order Generalized Integrator Frequency Locked Loop (DSOGI-FLL) in the proposed control system. All the works presented above were concentrated on the grid connected power converters with L and LC filter, while the vast mainstream of converters in RES applications use an LCL filter. Only the works in [10-12] have previously considered the VF-based voltage sensorless grid synchronization with LCL-filters. Thus, the work in [13] is the enhanced version of the work presented in [8] where the VF estimation is done by taking into consideration that the inverter is connected to the grid through the LCL filter.

This paper goes further from the analysis done in [13] where the control method presented is able to control the power injection not only at the second inductor of the filter, but also in a remote point of the line where it is connected, thus also extending the work done in [8, 9]. The control system will be implemented in the stationary reference frame and the PR current controller will be comprised in the inner loop control of the power converter. The work starts with an overview of the proposed control methods. It will be continued with an explanation of VF estimation for the case of LCL filter. Then, the experimental results are presented to validate the proposed system before concluding the paper with a discussion of obtained performance.

II. PROPOSED CONTROL METHOD BASED ON VF ESTIMATION

The framework that will be considered in this paper is shown in Fig. 1. The point of synchronization in previous works is normally located at the primary of the transformer, T_1. As a difference, in this paper, the VF estimation point is considered to be after the transformer, T_2.

This work has been partially supported by the Spanish Ministry of Innovation and Competitiveness under the project ENE2016-79493-R and ENE2017-88889-C2-1-R.

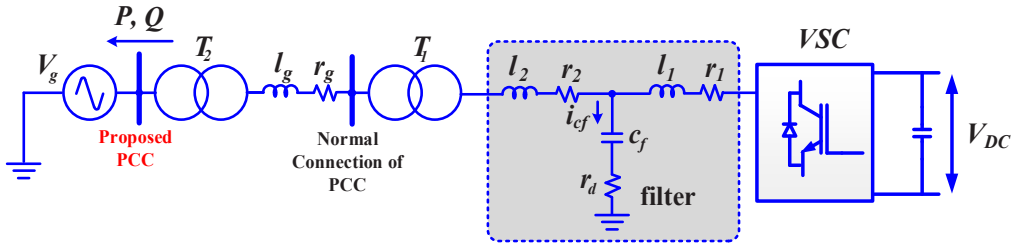

Fig. 1. Framework of investigated system

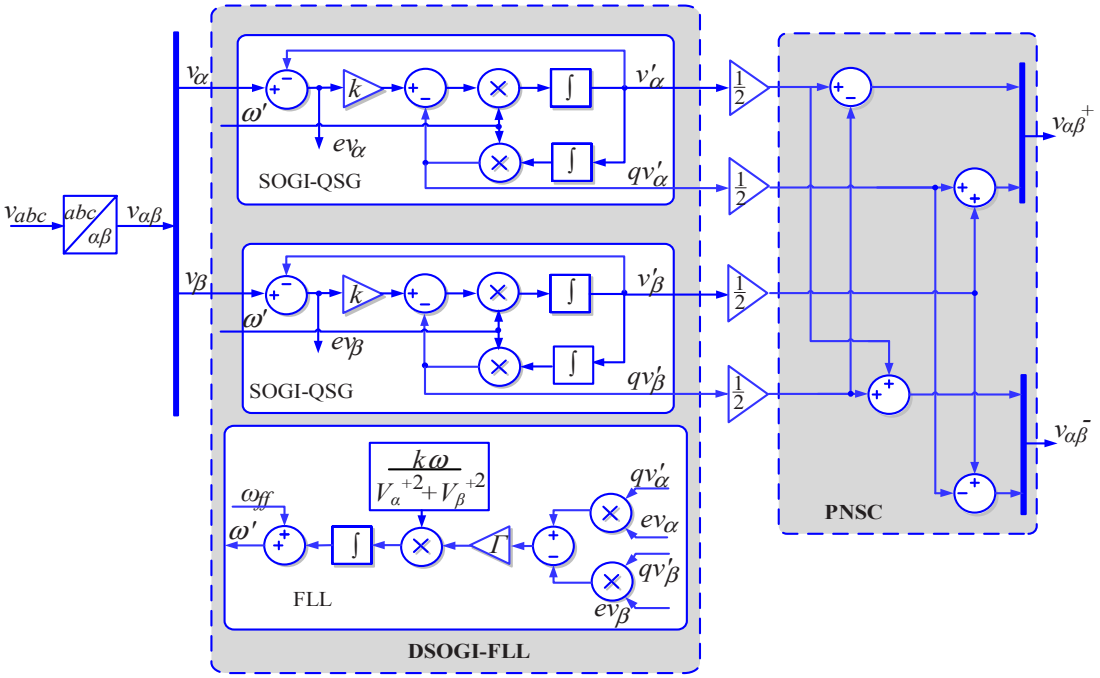

Fig. 2. Basic structure of a dual second order generalized integrator-based quadrature signal generator with frequency locked loop and PNSC

As a result, the VF estimation is possible to control the active and reactive power at the connection transformer that interfaces a plant with the main grid. The connection transformer can be located some kilometres away from the converter; hence, the control proposed in this paper permits to regulate the power delivery in a remote point. A virtual flux, Ψ, can be obtained by integrating the converter output voltage, V_{conv}.

The converter output voltage can be easily estimated by multiplying the DC-link voltage with the pulse width modulation reference signal of the converter, $m_{ref,\alpha\beta}$. Before performing the integration of the converter output voltage, the voltage drop caused by the conduction losses of the converter and the primary filter inductor, represented by the equivalent resistance r_1, should be taken into account. The virtual flux in stationary reference frame, $\alpha\beta$, can be determined in (1).

$$\Psi_{\alpha\beta}(t) = \int V_{conv}\,dt + \Psi_0 = \int m_{ref,\alpha\beta}\left(\frac{V_{dc}}{2}\right)dt + \Psi_0 \qquad (1)$$

In VF estimation, the ideal integration shown in (1) can be sensitive to drifts and offsets. In order to overcome this issues, a Dual Second Order Generalized Integrator based Quadrature Signal Generator (DSOGI-QSG) is used because it has a good filtering effect and allow to obtain the quadrature signals. The frequency input needed by the DSOGI-QSG is obtainable from the Frequency Locked Loop (FLL) output. The advantage of using the FLL is that; the system will be adapted to the center frequency of the SOGI resonators. As a result, overall DSOGI-QSG structure will be automatically adapted to the grid frequency variations.

The dual SOGI-QSG configuration considering the FLL as well as the Positive and Negative Sequence Components (PNSC) extractor is shown in Fig. 2. The configuration of the PNSC used in this work is the same configuration presented in [2]. As shown in Fig. 2, the SOGI-QSG provides a set of orthogonal signal *v-qv* with no necessity of using any phase angle to synchronize the input signal. Since both SOGIs are working at the same frequency, only one FLL will be used in the VF estimation. Considering the SOGI-QSG block in Fig. 2, the *v'* can be described as the direct output signal from the input signal *v* whereas *qv'* represents the in-quadrature output signal from *v'*, which is lagged by 90°. The *qv'* is in fact an integral of the output *v'* multiplied with the frequency *ω'*.

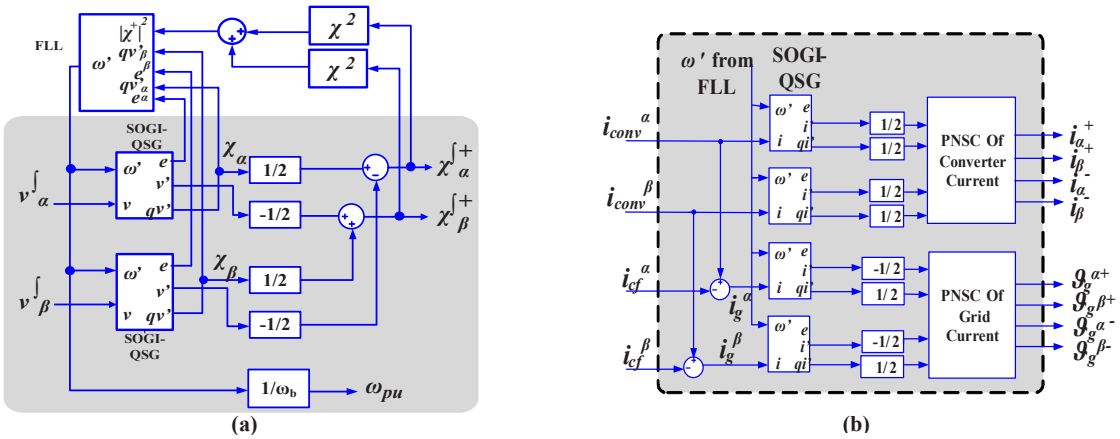

Fig. 3 (a) Positive sequence of virtual flux, (b) Sequence separation of converter currents and the grid current integral.

If the input v_α and v_β are considered as the input signals, the direct output signal v_α' and v_β' as well as the in-quadrature output signals, qv_α' and qv_β' are the filtered components of the signals, where in this case, the v_α' and v_β' are in phase with v_α and v_β. Similarly, the in-quadrature output signals, qv_α' and qv_β' are lagged by 90° with respect to the v_α' and v_β'. The error signals, ev_α and ev_β are measured between the input, v and the direct output, v', for both α and β components. Considering a constant resonance frequency, ω', the transfer function of the direct output signal v' with respect to the input v and the in-quadrature output signal qv' with respect to v' is given by (2) and (3), respectively.

$$\frac{v'}{v}(s)=\frac{k\omega' s}{s^2+k\omega' s+\omega'^2} \tag{2}$$

$$\frac{qv'}{v}(s)=\frac{k\omega'^2}{s^2+k\omega' s+\omega'^2} \tag{3}$$

The frequency response of the transfer functions given in (2) and (3) are shaped by the value of the gain constant, k. A good trade-off between overshoot and stabilization time will be obtained by selecting the gain constant, $k=\sqrt{2}$. For this reason, $k=\sqrt{2}$ will be used in the experimental validation. By referring to the transfer function stated in (2), it can be concluded that the direct output voltage v' has band pass characteristics with unitary gain and zero phase shift at the fundamental angular frequency, ω_0. On the other hand, the transfer function stated in (3) has a low pass characteristic with unitary gain and −90° phase shift at the fundamental frequency.

III. Implementation Of VF Estimation With LCL Filter

A. Voltage Sensor-less VF Estimation

In this work, the controlled current is based on the current measurement at the converter side, i_{conv}. Since the system is working in the stationary reference frame, the three phase quantities of the converter output current must be transformed into the alpha-beta domain. Based on the equation shown in (1), the flux is achieved by integrating the converter voltage. As explained in section II, the voltage to be integrated is actually the compensated converter output voltage, $v^{\int}_{\alpha\beta}$, which is found considering the subtraction of the resistive voltage drop at r_1 from the converter's output voltage. This compensated converter output voltage is given in (4).

$$v^{\int}_{\alpha\beta}(t)=\left[\left(m_{ref}{}^{\alpha\beta}\cdot v_{DC}\right)-\left(r_1\cdot i_{conv}{}^{\alpha\beta}\right)\right]dt \tag{4}$$

The direct output voltage, v' of the SOGI-QSG provides 90° phase shifted for the sequence separation. Considering that the output is the derivative of VF, changing the sign will be equal to a 90° phase lag. Taking into consideration the per unit values used, the virtual flux later can be expressed as χ. The positive and negative sequence of VF can be obtained by using the PNSC block as shown in Fig. 2. Since the positive sequence of VF estimation will be used later in calculating the current reference, Fig. 3(a) shows the method of obtaining only the positive sequence of the virtual flux while the sequence separation of the converter and the integral of the grid current are shown in Fig. 3(b). Since the control strategy is based on the voltage sensorless concept, the capacitor voltage, v_{cf} is essential to be estimated in order to estimate the capacitor current, i_{cf}. Considering the use of per unit frequency, ω_{pu} in the estimation, the capacitor voltage in $\alpha\beta$ components can be obtained by (5).

$$\begin{aligned} v_{cf}{}^{\alpha}(t)&=\left(\left(v^{\int}{}_{\alpha}\right)dt\cdot\left[\left(\omega_{pu}\cdot l_1\right)\cdot\left(i_{conv}{}^{\beta}(t)\right)\right]\right)\\ v_{cf}{}^{\beta}(t)&=\left(\left(v^{\int}{}_{\beta}\right)dt\cdot\left[\left(\omega_{pu}\cdot l_1\right)\cdot\left(i_{conv}{}^{\alpha}(t)\right)\right]\right)\end{aligned} \tag{5}$$

The positive and negative sequence of VF estimation at the filter capacitor can be found in (6) where $\chi^{\int}_{\alpha\beta}{}^{+-}$ is the output of DSOGI-VF in both positive and negative sequence. It can be seen in this equation, the inductive flux drop across l_1 has been subtracted from the obtained virtual flux, $\chi^{\int}_{\alpha\beta}{}^{+-}$.

$$\chi_c^{\alpha\beta+-}(t)=\underbrace{\left[\int\left(m_{ref}{}^{\alpha\beta+-}\cdot v_{dc}-r_1\cdot i_{conv}{}^{\alpha\beta+-}(t)\right)\right]}_{\chi^{\int}_{\alpha\beta}{}^{+-}}-l_1\cdot i_{conv}{}^{\alpha\beta+-}(t) \tag{6}$$

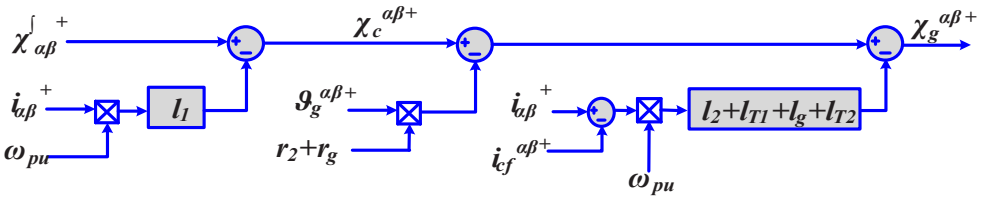

Fig. 4. Virtual flux estimation at the grid side.

Since the VF estimation at the filter capacitor is available in (6), the positive and negative sequence of the capacitor current can be estimated based on this flux estimation. The voltage drop at the grid side is calculated by multiplying the integral of the grid current, $\vartheta_g^{\alpha\beta}$ with the added value of r_2 and r_g. The inductive fluxes drop at the grid side have been considered by multiplying the grid current by the addition of l_2, l_{T1}, l_g and l_{T2}. The values of l_{T1} and l_{T2} on the other hands are the 3% of the transformer base impedance, namely Z_{T1} and Z_{T2} where the rated power of the transformer T_1 and T_2 used in the lab are 20 kVA. The resulting of VF estimation at the grid side considering only the positive sequence is given by (7).

$$\chi_g^{\alpha\beta+}(t)=\chi_c^{\alpha\beta+}(t)-\left(r_2+r_g\right)\cdot\vartheta_g^{\alpha\beta+}(t)-(l_2+l_{T1}+l_g+l_{T2})\cdot i_g^{\alpha\beta+}(t) \tag{7}$$

In this case, the grid current has been obtained by subtracting the capacitor current from the converter current in both alpha and beta component. The positive sequence coming from the VF estimation at the grid side in (7) is shown graphically in Fig. 4.

B. Filtering Configuration

In this work, a passive damping has been considered for the LCL filter, thus, the damping resistors are placed in series with the capacitor branch. Taking into consideration the per phase model of the LCL filter shown in Fig. 1, the transfer functions considering two scenarios: with and without the damping resistor are given by (8) and (9) respectively.

$$G_{F,d}(s)=\frac{C_f R_d s+1}{L_1 C_f L_2 s^3+C_f(L_1L_2)R_d s^2+(L_1+L_2)s} \tag{8}$$

$$G_F(s)=\frac{1}{L_1 C_f L_2 s^3+(L_1+L_2)s} \tag{9}$$

The idea of having the damping resistor in the design shown in (8) is to smoothen the spike that appears in (9) when considering only inductive and capacitive elements in the filter transfer function. In order to have a more realistic approach, the damping resistor will be considered as a former element in the study case from now on. The LCL-filter parameters and other operating nominal values used for the experimental studies are listed in Table I.

TABLE I. SYSTEM PARAMETERS

Abbreviation	*Nomenclature*	*Values*
S_N	Rated Apparent Power	10 kVA
f_{sw}	Switching Frequency	10 kHz
$V_{g(p\text{-}p)}$	Phase to Phase Grid Voltage	380 V
$V_{g(p)}$	Phase Voltage	230 V
V_{DC}	DC-Link Voltage	700 V
$l_{1(abc)}$	Inductor, l_1	3.4 mH
$l_{2(abc)}$	Inductor, l_2	0.588 mH
$l_{g(abc)}$	Grid Inductance, l_g	10 mH
$c_{f(abc)}$	Filter Capacitor	4.7 µF
$r_{d(abc)}$	Damping Resistor	1.8 Ω

C. Inner Loop Control of the VSC and Current Reference Generation

For the grid tied inverter, the accuracy of the inner loop control is very important. In this work, the PR current controller will be used to accommodate the inner loop control of the VSC. This selection is supported by the fact that the PR current controller offers a very good performance and the implementation is not complex. An ideal PR controller is described in (10). However, in the real implementation, it may give stability problems due to its infinite gain.

$$G_{PR}(s)=K_p+K_r\frac{s}{s^2+\omega_o^2} \tag{10}$$

In order to avoid this issues, the PR controller can be made as non-ideal, considering a damped or bandpass structure in its implementation. The resulting transfer function for the non-ideal case is given by (11):

$$G_{PR}(s)=K_p+K_r\frac{2\omega_c s}{s^2+2\omega_c s+\omega_o^2} \tag{11}$$

The bandwidth in the transfer function shown in (10) is very small and almost null if compared to the non-ideal cases shown in (11), where the ω_c can be used to control the bandwidth. The gain of the PR controller at the frequency ω_o in (11) is finite, but it is still capable to provide only a very small/null steady state error. This is the reason that makes the controller reliable when it is digitally implemented in the real applications. In both (10) and (11), the K_p is the proportional gain and K_r is the resonant gain term. The ideal resonant provides an infinite gain at the ac frequency ω_o and no phase shift and gain at the other frequencies. In the case of non-ideal PR controller, the smaller the value of ω_c, the more sensitive the filter to the frequency variations. Besides that, it will also leads to a slower transient response. Normally, a reasonable value of ω_c used in practice is between 5–15 rad/s.

In this controller, it is also possible to control the bandwidth by using the K_r value. A larger bandwidth can be obtained with a higher values of K_r, but the stability of the system should be taken into account in selecting this gain. On the other hand, by varying the value of K_p, it will affect the magnitude. The magnitude increases with K_p but the peak value is still at the resonant frequency The output of the PR current controller is the reference voltage needed at both α and β components.

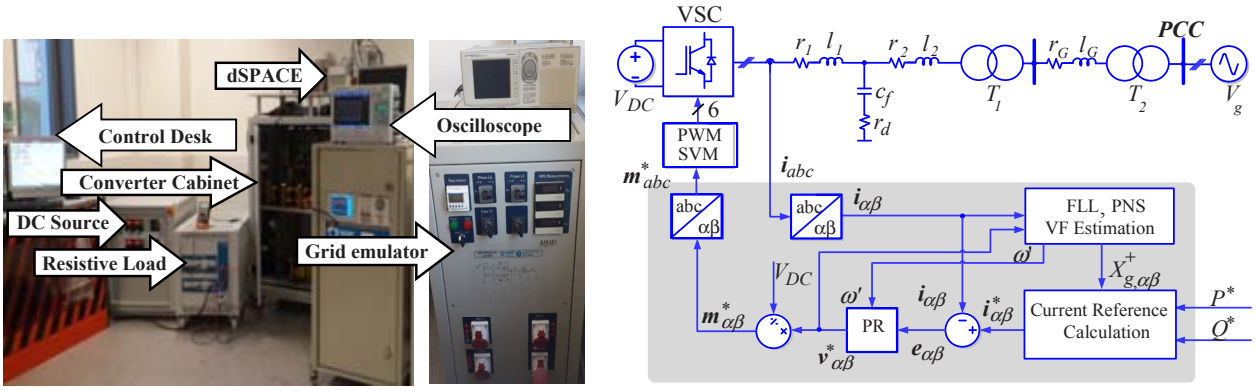

(a) **(b)**

Fig. 5 (a) Experimental setup in the lab, (b) Structure of the study case considered for the experimental validation

The modulation index, $m_{ref,\alpha}$ and $m_{ref,\beta}$ used in calculating the converter voltage can be obtained by dividing the reference voltage, $v^*_{\alpha\beta}$ by the V_{DC}. This modulation index then will be transformed into the *abc* reference frame.

Besides the current controller and the VF estimation, it is also essential to determine the set point to be provided to the current controller. This set point is known as a current reference. The current reference is the output generated by the outer loop controller. The current reference used in this work is calculated based on the power calculation where the active and reactive power reference are also required in the calculation. To make it significant to the proposed method, the positive sequence of the VF estimation at both alpha and beta components also will be used to calculate the current reference. Therefore, a reliable VF estimation is very important in this case. Any errors in the VF estimation will directly affect the tracking capability of the system. Since the current is controlled at the converter side, the capacitor current needs to be added with the current at PCC in order to match with the current at the converter side. The current references in the alpha and beta reference frame can be calculated by using (12) and (13).

$$i_\alpha^* = \left[\frac{P_{ref}\cdot\chi_g^{\alpha+} + Q_{ref}\cdot\chi_g^{\beta+}}{\chi_g^{\alpha+^2} + \chi_g^{\beta+^2}}\right] + i_f^{\ \alpha} \tag{12}$$

$$i_\beta^* = \left[\frac{P_{ref}\cdot\chi_g^{\beta+} + Q_{ref}\cdot\chi_g^{\alpha+}}{\chi_g^{\alpha+^2} + \chi_g^{\beta+^2}}\right] + i_f^{\ \beta} \tag{13}$$

IV. Experimental Validation of the Proposed System

The experimental setup used in the lab is shown in Fig. 5(a) while the structure of the overall study case is shown in Fig. 5(b). The arrangement for the experimental validation consists of a 10 kVA inverter which is linked to a controlled 230 V phase-to-phase (400 V line-to-line), 50 Hz three phase AC power source through the LCL filter. The inverter has been powered by a programmable dc power supply that provides a 700 V_{DC}-link. The inverter, LCL filter and the transformer are located inside the converter cabinet and the output from the converter is connected to the input of the oscilloscope. The output of the oscilloscope then will be linked to the grid emulator-sag generator device, which supplied the grid voltage to the overall system.

The proposed control method has been programmed on a dSpace1103 platform. A grid inductance value used in this test has been set to 10mH. The setting of the grid inductance value is available from the "grid emulator-voltage sag generator device". The measured and estimated signals has been plotted using SCADA system which is built using the Control Desk application of dSpace. By using the control desk application, the active and reactive power references can be changed accordingly and all the signals are easily managed.

The experimental studies have been conducted based on the structure shown in Fig. 5 and the system parameters listed in Table I. In the first study case, the active power reference is set from 0 to 8kW, which in this case is equivalent to 0.8 p.u. The reactive power reference on the other hands is set as 0 kVar. The experimental results captured form the control desk is presented in Fig. 6 with the K_p and K_r values have been set to 7 and 19 respectively.

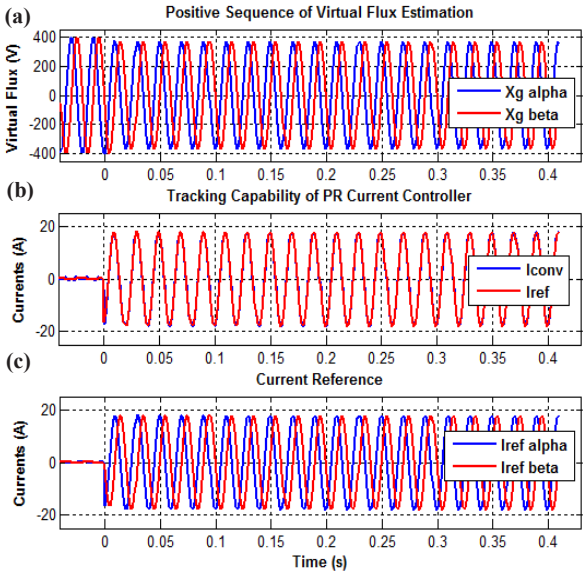

Fig. 6. Experimental results captured from the dSpace control desk; (a) Positive sequence of virtual flux estimation, (b) Tracking capability of PR current controller, (c) Current reference generation

Based on the results obtained, it is clearly shown that the VF based synchronization method works as it should be without measuring the grid voltage for the synchronization process. The results shown in Fig. 6 shows that the system is working perfectly without any issues during the transient state as well as in the steady state conditions. Considering the test is performed under balance condition, it is clear that the positive sequence of the VF estimation has the same amplitude, as shown in Fig. 6(a). The VF estimation at the grid side reached 380V when the V_{DC} and V_{AC} are at the maximum value as stated in Table I. As expected, the VF estimation at the beta component lags the alpha component by 90°.

The PR current controller is working adequately where in this case, the converter current is able to follow the reference current without any delay or phase displacement as shown in Fig. 6(b). This result prove that the PR current controller is effective to control the currents as the tracking capability is really good. It is worth to mention here that there is no voltage feedforward considered in the proposed system.

The current reference used for the PR current controller is balanced and has the same amplitude as shown in Fig. 6(c). In this regards, the results shown in Fig. 6(a) really has a big influence to the plot shown in Fig. 6(c) because the positive sequence virtual flux estimation has been used in calculating the current reference. If the VF estimation at the grid side condition is not balance, the amplitude of the current reference surely will be affected thus influence the tracking capability of the system.

In Fig. 7(a) and Fig. 7(b), it show that the active and reactive power measurements are matched with the active and reactive power reference that have been set earlier.

The capability of PR current controller to eliminate the tracking error is proved in Fig. 7(c) where it can be clearly seen in this plot that the error in the α and β components are zero during the steady state condition.

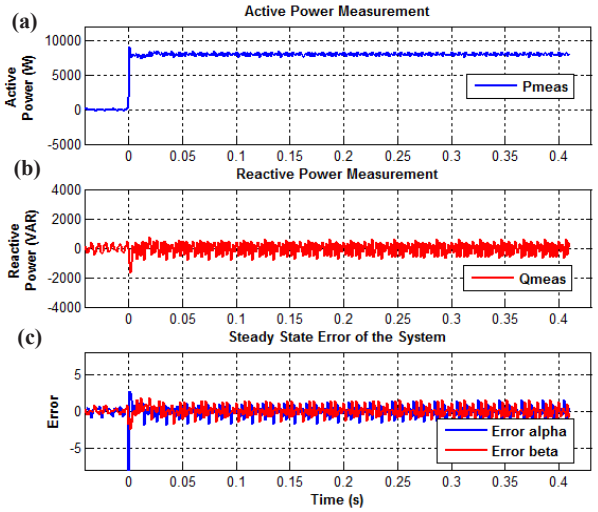

Fig. 7. Active power change; (a) Active power measurement, (b) Reactive power measurement, (c) Steady state error of the system.

In the 2nd study case, 7.5kW (0.75 p.u) and 6 kVar (0.6 p.u) have been injected to the grid and the results captured from the oscilloscope is shown in Fig. 8(a) and Fig. 8(b) respectively. The results shown in Fig. 8 are reasonable and satisfactory when taken into account the power losses occurred during the experimental. A very smooth transient state condition of both active and reactive power injection also can be seen in this plot. Since the frequency is the most important global magnitude in AC network, it should be ideally maintained by all the interrelated elements in a cooperative manner. In the case of the frequency variations, regulating the active power is essential by means of increasing/decreasing the power when the frequency is decrease/increase.

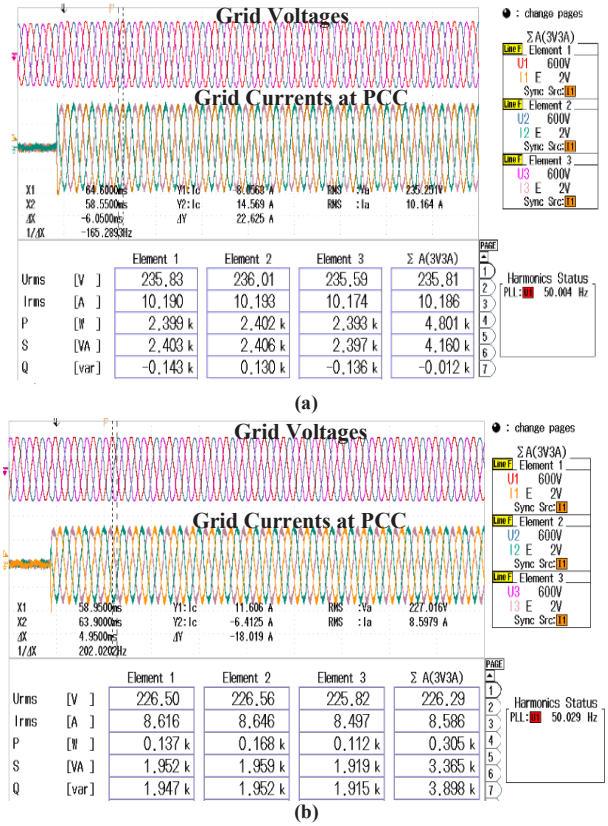

Fig. 8. Change in active power and reactive power, (a) Reference step is set from 0 to 7.5kW (0.75 p.u), (b) Reference step is set from 0 to 6 kVar (0.6 p.u).

The zoom version of the grid voltages and currents at the PCC is shown in Fig. 9. The system is working very well without any transient overshoot when the step reference has been applied as shown in Fig. 9(a). Fig. 9(b) is the zoom version of the waveforms shown in Fig. 8(b). By referring to the red box in Fig. 9(b), it can be seen that the current, I1 lags the voltage, U1 by almost 90° when purely reactive power is injected. The system is working at 50 Hz fundamental frequency and the time for one full cycle is equal to 20 ms. Since one full cycle is equivalent to 360°, $\Delta X = 4.95$ ms is considered as 89.1° phase lag [(360° × 4.95 ms)/20 ms.

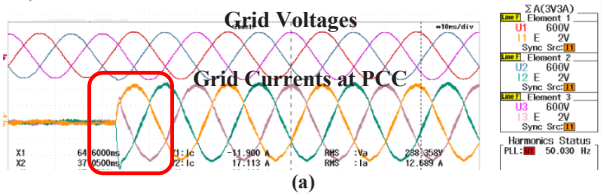

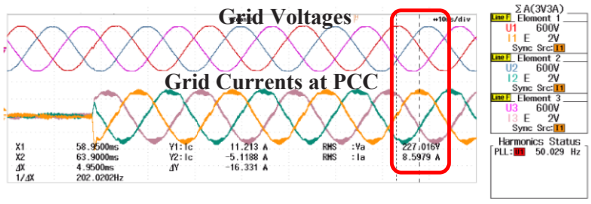

(b)

Fig. 9. Grid voltages and currents at PCC; (a) Grid voltages and currents when the step reference from 0 to 10kW has been applied, (b) Injection of reactive power when step change has been applied from 0 to 6 kVar (0.6 p.u).

V. Conclusion

This paper presented a control method which is relied on the VF based synchronization. The control strategies presented permit to control the active and reactive power delivery in a remote point of the grid, as for an example, at the transformer connection point. In general, the presented results endorsed the accuracy of VF estimation, since the synchronization with the grid and the corresponding control of the active and reactive power injection to the PCC is based on the VF signals. Furthermore, a fast synchronization and a very smooth reference tracking has been achieved during the transient conditions. The most obvious finding is that the VF estimation is reliable to estimate the voltage at different points along the grid that make it possible to control the power injection/absorption remotely.

Acknowledgment

This work has been partially supported by the Spanish Ministry of Innovation and Competitiveness under the project ENE2016-79493-R and ENE2017-88889-C2-1-R. Any opinions, findings, and conclusions or recommendations expressed in this material are those of the authors and do not necessarily reflect those of the host institutions or founders.

References

[1] IRENA. "REthinking Energy 2017: Accelerating global energy transformation, International Renewable Energy Agency (IRENA)," http://www.irena.org/DocumentDownloads/Publications/IRENA_REthinking_Energy_2017.pdf.

[2] A. Luna, J. Rocabert, J. Ignacio Candela, J. R. Hermoso, R. Teodorescu, F. Blaabjerg, and P. Rodriquez, "Grid voltage synchronization for distributed generation systems under grid fault conditions," *IEEE Transactions on Industry Applications,* vol. 51, no. 4, pp. 3414 – 3425, 2015.

[3] S. Hansen, M. Malinowski, F. Blaabjerg, and M. P. Kazmierkowski, "Sensor-less control strategies for PWM rectifier," in Proceedings of the 15th Annual IEEE Applied Power Electronics Conference and Exposition, New Orleans, Louisiana, 2000, pp. 832–838.

[4] M. Malinowski, M. P. Kazmierkowski, S. Hansen, F. Blaabjerg, and G. D. Marques, "Virtual-flux-based direct power control of three-phase PWM rectifiers," *IEEE Transactions on Industry Applications,* vol. 37, no. 4, pp. 1019–1027, 2001.

[5] M. Malinowski, M. P. Kazmierkowski, and A. M. Trzynadlowski, "A comparative study of control techniques for PWM rectifiers in AC adjustable speed drives," *IEEE Transactions on Power Electronics,* vol. 18, no. 6, pp. 1390–1396, 2003.

[6] J. G. Norniella, J. M. Cano, G. A. Orcajo, C. H. Rojas, J. F. Pedrayes, M. F. Cabanas, and M. G. Melero, "Improving the dynamics of virtual-flux-based control of three-phase active rectifiers," *IEEE Transactions on Industrial Electronics,* vol. 61, no. 1, pp. 177–187, 2014.

[7] A. Kulka, "Sensor-less digital control of grid connected three phase converters for renewable sources," Ph.D Dissertation, Norwegian Univ. Sci. Technology, Trondheim, Norway, 2009.

[8] J. A. Suul, "Control of grid integrated voltage source converters under unbalanced conditions – Development of an online frequency adaptive virtual flux based approach," Ph.D Dissertation, Norwegian Univ. Sci. Technology, Trondheim, Norway, 2012.

[9] J. A. Suul, A. Luna, P. Rodríguez, and T. Undeland, "Voltage-sensor-less synchronization to unbalanced grids by frequency-adaptive virtual flux estimation," *IEEE Transactions on Industrial Electronics,* vol. 59, no. 7, pp. 2910–2923, 2012.

[10] J. Zhang, H. Wang, M. Zhu, and X. Cai, "Control implementation of the full-scale wind power converter without grid voltage sensors," in Proceedings of 2014 International Power Electronics Conference, Hiroshima, Japan, 2014, pp. 1753-1760.

[11] G. Wrona, and K. Malon, "Sensorless operation of an active front end converter with LCL filter," in Proceedings of 2014 IEEE 23rd International Symposium on Industrial Electronics, ISIE 2014, Istanbul, Turkey, 2014, pp. 2697-2702.

[12] W. Gullvik, L. Norum, and R. Nilsen, "Active damping of resonance oscillations in LCL-filters based on virtual flux and virtual resistor," in Proceedings of 12th European Conference on Power Electronics and Applications, Aalborg, Denmark, 2007, pp. 1-10.

[13] N. F. Roslan, J. A. Suul, J. Rocabert, and P. Rodriguez, "A Comparative study of methods for estimating virtual flux at the point of common coupling in grid-connected voltage source converters with LCL filter," *IEEE Transactions on Industry Applications,* vol. 53, no. 6, pp. 5795-5809, 2017.